REMARKS

Claims 1-19 are pending in the present application. Claims 1-8 are withdrawn. Claim 15 is herein amended.

Specification Objection

The title of the invention was objected to for lack of descriptiveness. The title of the invention has been amended to clearly indicate the invention to which the claims are directed. Withdrawal of the objection is requested.

Claim Rejections - 35 U.S.C. § 103

Claims 9-19 were rejected under 35 U.S.C. § 103(a) as being unpatentable over ***Kishi*** (U.S. Patent 6,133,605). Favorable reconsideration is requested.

Claims 9 and 12 recite a manufacturing method of a semiconductor device. The manufacturing method includes steps for forming a gate insulation film. The steps include forming a silicon oxide film over the silicon substrate and introducing nitrogen into the silicon oxide film for displacing silicon atoms on a surface of the silicon substrate towards the gate insulation film side. The claims recite the silicon oxide film having a thickness of 1.5 nm or less.

Applicants respectfully submit that it would not have been obvious to one of ordinary skill in the art to use a silicon oxide film having a thickness of 1.5 nm or less from the teachings of *Kishi*. The use of a silicon oxide film of 1.5 nm or less provides unexpected results.

The enclosed reference, **Awaji**, *High-Precision X-Ray Reflectivity Study of Ultrathin SiO_2 on Si*, J. Vac. Sci. Technology A., vol. 14, no. 3, pp. 971-976, May 1996 ("*Awaji*"), discloses a silicon oxide film whose thickness is 4.0 nm and has an interfacial layer on a surface of a substrate and a SiO_2 layer thereon. The interfacial layer has a thickness of 0.8 to 1.4 nm

(roughness of 0.4 nm). The density between these two layers is different. Also, while the bonding condition in the SiO_2 layer is almost perfect and strong, the bonding condition in the interfacial layer is imperfect.

The thickness of the interfacial layer in a silicon oxide film formed by thermal oxidation is constant no matter how thick the silicon oxide film is. Therefore, when the thickness of a silicon oxide film is 1.5 nm or less, as in the present invention, the whole film is the interfacial layer. On the other hand, in *Kishi*, the silicon oxide film has not only the interfacial layer but also the SiO_2 layer.

Accordingly, in the present invention, an intended strain can be generated by introducing nitrogen. In *Kishi*, on the other hand, the intended strain cannot be generated because of the SiO_2 layer, in which the bonding condition is complete in the silicon oxide film.

Behavior of a silicon oxide film (thickness of 2.4 nm) when it is nitrided in a NO gas atmosphere is described in the enclosed reference, **Takahashi**, *Novel Interface Structures between Ultrathin Oxynitride and Si(001) Studied by X-Ray Diffraction*, Jpn. J. Appl. Phys., vol. 42, pp. 7493-7496, Dec. 2003 ("*Takahashi*"). The paper describes that the crystal structure of the silicon oxide film changes as nitriding progresses. Therefore, nitrogen atoms introduced to a silicon oxide film affect not only the interfacial layer but also the SiO_2 layer. In other words, the nitrogen atoms collapse the crystal structure of the SiO_2 layer and bond to the collapsed SiO_2 layer before reaching the interfacial layer.

Accordingly, the effect and function of nitrogen atoms differs when the thickness of a silicon oxide film is 2.2 nm and when it is 1.5 nm. This is the case even if the same nitriding treatment is performed. In addition, the influence which affects the interface between a substrate

and the silicon oxide film differs between the two thicknesses. Therefore, it would not have been obvious to one of ordinary skill in the art to use a silicon oxide film having a thickness of 1.5 nm or less from the teachings of *Kishi*.

Accordingly, withdrawal of the rejection of claims 9-19 based on *Kishi* is hereby solicited.

Applicants also respectfully submit that *Kishi* does not disclose:

> forming a silicon nitride film or high dielectric constant film over said silicon oxide film by a deposition method, after said step of introducing nitrogen and displacing silicon atoms

as recited in amended claim 15.

When a silicon nitride film or high dielectric constant film is formed by a deposition method, nitrogen or the like is newly supplied. Therefore, the dielectric constant of the gate insulation film further increases. This makes it possible to make an electrical thickness of the gate insulation film thin, and to decrease leak current.

In *Kishi*, on the other hand, the oxygen-rich silicon nitrided oxide film 4 is formed by oxidizing a surface of the silicon nitrided oxide film. When forming the oxygen-rich silicon nitrided oxide film by oxidizing the surface, nitrogen is never supplied in the process. Therefore, the dielectric constant of the gate insulation film is not increased.

Kishi does not disclose forming a silicon nitride film by a deposition method. Therefore, *Kishi* does not recite the elements of claim 15.

Accordingly, withdrawal of the rejection of claim 15 based on *Kishi* is hereby solicited.

In view of the aforementioned amendments and accompanying remarks, Applicants submit that that the claims, as herein amended, are in condition for allowance. Applicants request such action at an early date.

If the Examiner believes that this application is not now in condition for allowance, the Examiner is requested to contact Applicants' undersigned attorney to arrange for an interview to expedite the disposition of this case.

If this paper is not timely filed, Applicants respectfully petition for an appropriate extension of time. The fees for such an extension or any other fees that may be due with respect to this paper may be charged to Deposit Account No. 50-2866.

Respectfully submitted,

WESTERMAN, HATTORI, DANIELS & ADRIAN, LLP

Andrew G. Melick
Attorney for Applicants
Registration No. 56,868
Telephone: (202) 822-1100
Facsimile: (202) 822-1111

AGM/sg
Enclosures: *Awaji* Article
Takahashi Article

Appendix A

High-precision x-ray reflectivity study of ultrathin SiO_2 on Si

N. Awaji, Y. Sugita, T. Nakanishi, S. Ohkubo, K. Takasaki, and S. Komiya
Fujitsu Laboratories Ltd., 10-1 Morinosato-Wakamiya, Atsugi 243-01, Japan

(Received 2 October 1995; accepted 26 February 1996)

We have developed a high-precision difference-x-ray-reflectivity technique using intense synchrotron radiation and applied this to evaluate native oxides and ultrathin thermal oxides on Si(100). We have successfully evaluated the density of native oxides. Native oxides formed by HCl and NH_4OH solutions have a low density, in contrast to the oxides formed by H_2SO_4 solution and UV/O_3 whose densities are close to those of thermal oxides. By carefully analyzing ultrathin thermally grown oxides with thicknesses of 40 and 70 Å grown at 800–1000 °C, we have revealed the existence of a dense (~2.4 g/cm³), thin (~10 Å) layer at the SiO_2/Si interface. Oxides grown in O_3 or HCl/O_2 have a thinner interfacial layer compared to those grown in O_2. We have evaluated the effects of ambient and temperature at oxidation on the interfacial layer and the SiO_2 layer.

I. INTRODUCTION

The current trend toward increased density of ultralarge scale integrated devices has required highly reliable ultrathin SiO_2 gates as thin as 40 Å. For such ultrathin oxides, characterizations of the initial surface before oxidation, along with the structure at the SiO_2/Si interface for the grown oxide, are important issues. X-ray reflectivity technique offers a powerful tool to evaluate the density, thickness, and surface and interface microroughness for multilayer thin films, with a well-established theoretical basis.[1–4] However, application of the techniques to SiO_2 on Si (Refs. 5 and 6) has not been popular since the closeness of the density of SiO_2 to that of the Si substrates leads to a weak oscillation fringe superimposed on a rapidly decreasing reflectivity intensity, which made detailed evaluation difficult. Also the dynamic range of measurement was not enough to evaluate the structure at around 10 Å. Recently, we developed high-precision difference-x-ray-reflectivity (DXR) techniques using the intense synchrotron radiation that enables the detailed evaluation of ultrathin SiO_2 on Si.

II. EXPERIMENT

The x-ray reflectivity is measured using synchrotron radiation at beamline 17 C Photon Factory (PF) KEK using a grazing incidence x-ray diffractometer.[7] An x-ray wavelength of 1.3 Å was chosen by the Si(111) double crystal monochrometer for measurements. Highly parallel, intense synchrotron radiated x rays are applied with an incident collimating slit of 100 μm and a reception slit of 200 μm before the NaI counter. An aluminum absorber is placed after the monochrometer to attenuate the incident x ray by 1/1000 to avoid saturation of the counter for measurement at the incident angle ψ, defined by the angle between an incident x ray and the sample surface, below 0.5°. The typical counting rate of reflectivity was 2×10^8 cps at a low incident angle, after correcting the absorber, and the background count was 8 cps. This provided more than 10^7 intensity range of reflectivity. The corresponding scattering angle, 2ψ, extended up to around 9°.

The measured reflectivity is usually compared directly to the model calculation. However, to see the contribution of such thin layers more clearly, we defined the DXR. The DXR (denoted by ΔR) is obtained by subtracting the average log reflectivity, $\log R_{ave}$, from the measured log reflectivity, $\log R$, of the sample as follows:

$$\Delta R = \log(R/R_{ave}).$$

R_{ave} must be clearly defined and has no oscillatory behavior. It is not difficult to mathematically confirm that if the refractive index of the thin film and the substrate are similar, the global structure of reflectivity can be canceled out by applying the reflectivity of the substrate as the R_{ave}, and ΔR provides the interference fringe originated from the ultrathin layer. As described later, term R_{ave} is subtracted out from both measured and calculated reflectivity the same way. In this case, the contribution of subtracted R_{ave} in the least square function χ^2, defined below, is totally canceled out and the nonsubtracted χ^2 results. Hence, no additional inaccuracy has been introduced by this subtraction in the least square analysis. The advantage of the difference method is much clearer during minimization, such as initial parameter setting or convergence criteria and the appropriateness of the model.

The reflectivity can be calculated from Snell's law based on the complex refractive index $n = 1 - \delta + i\beta$ of the materials, which is proportional to the density of the materials in the hard x-ray regime.[1] We developed the optimization program based on the Marquardt minimization procedure for the extraction of film parameters. The reflectivity is calculated based on the Vidal and Vincent formalism.[2] In the model, the Gaussian rms microroughness of the sample surface and the interfaces between layers are fully considered.[3,4] The complex refractive index of materials is obtained from the table of atomic scattering factors by Henke *et al.*[8] and Sasaki.[9]

III. NATIVE OXIDES

CZ-Si(100) wafers were cleaned using H_2SO_4/H_2O_2 followed by dipping in 5% HF solution to remove chemically formed oxides. The wafers are processed by the following

 0734-2101/96/14(3)/971/6/$10.00

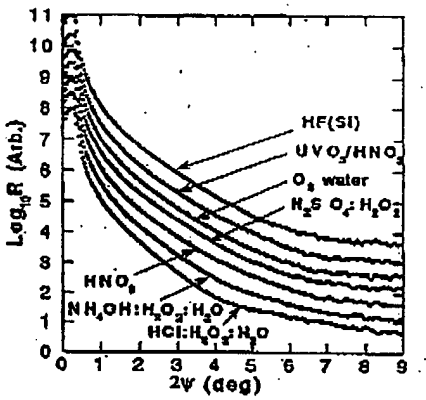

FIG. 1. Experimental x-ray reflectivity from native oxides formed by various chemical solutions. The reflectivity of the Si wafer after removing the HCl-formed native oxide by HF dip is also shown for reference. For clarity, each curve has been displaced vertically by 0.5.

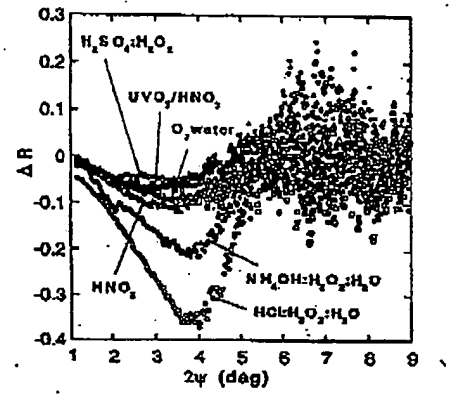

FIG. 2. Difference x-ray reflectivity, obtained by dividing the reflectivity of native oxide by that of HF-treated Si wafer, for various chemically formed samples.

various chemical treatments: boiled HCl solution (7%HCl–5%H_2O_2), boiled NH_4OH solution (4%NH_4OH –8%H_2O_2), boiled H_2SO_4 solution (83%H_2SO_4 –4%H_2O_2), boiled HNO_3 solution (61%HNO_3), O_3–water,[10] and UV/O_3 treatment.[11,12] The O_3–water sample was formed by rinsing the HF dipped wafers for 10 min in 18 ppm O_3–water produced by electrolysis. The UV/O_3 samples were prepared by transferring the boiled HNO_3 wafers in a quartz chamber, in which a highly purified oxygen gas flows (2 slm), containing 5% ozone produced by a discharge-type ozonizer, with irradiation by a mercury tube for 5 min.

For each condition, more than two wafers were prepared and the reflectivity was measured to confirm the repeatability of the result. After the measurements, native oxides at the sample surface were removed by 5% HF dipping for 5 min. The reflectivity of such hydrogen-terminated Si wafers was also measured and used as the average reflectivity, R_{ave}.

Figure 1 shows the measured reflectivity of native oxides formed by various chemical treatments, along with that of Si wafers after removing the HCl-formed native oxide by HF treatment. The DXRs of the measured samples are shown in Fig. 2. The interference fringes of native oxides are clearly visible, with a significant difference in the fringe intensity for each chemically treated sample.

The upper part of Fig. 3 shows the calculation of DXR for the typical 10 Å native oxides with surface and interface roughnesses of 3 and 2 Å, respectively. The assumed densities of oxides in Fig. 3 are from 1.9 to 2.3 g/cm^3. From comparing the calculated to the measured data, it is clear that the densities of native oxides depend on the chemical solutions used. The dip position of the interference fringe closely relates to the thickness of the native oxide. By this comparison, the thickness of native oxides formed during chemical treatments are almost the same.

In the analysis, the reflectivity of HF-dipped Si wafers was analyzed by the model, assuming only a Si substrate. The density of the Si wafer extracted by optimization was consistent with the known value of 2.33 g/cm^3 within a margin of error, and it was fixed at this value during the following analysis. The fitted roughness of HF-treated Si wafers are summarized in column $\sigma_{s,HF}$ in Table I. In the next stage, the DXR was analyzed by minimizing the error function defined as

$$\chi^2=\Sigma(\Delta R_{data}-\Delta R_{calc})^2/w^2,$$

where ΔR_{data} and ΔR_{calc} are the measured and calculated DXR intensities of the native oxide, respectively, and w is the weight for each data point. The resultant parameters are summarized in Table I.[13] The attached errors on the extracted parameters took into account that of least square minimization and the reproducibility of the result.

The thickness of the native oxide was around 10 Å with a slightly thick value for the UV/O_3 treatment sample. In terms of the density, the native oxides formed by boiled HCl and boiled NH_4OH solutions are less dense compared to those of

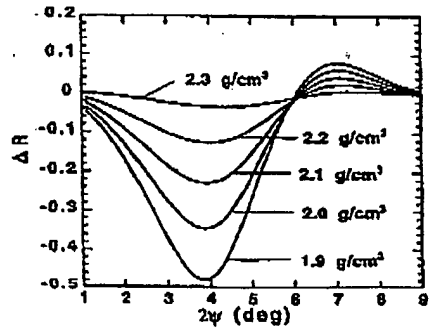

FIG. 3. Calculated difference x-ray reflectivity for the typical 10 Å native oxides with a surface and interface roughness of 3 and 2 Å, respectively. The density of the oxide is 1.9–2.3 g/cm^3.

TABLE I. Parameters of native oxides extracted from the fit. σ_s and $\sigma_{s,HF}$ indicate the surface roughness of native oxide and that of HF-treated Si wafers, respectively. σ_I indicates the interface roughness at Si substrate.

Sample	Oxide thickness(Å)	Density (g/cm^3)	σ_I (Å)	σ_s (Å)	$\sigma_{s,HF}$ (Å)
$HCl:H_2O_2:H_2O$	11.3	2.07	2.1	3.6	3.1
$NH_4OH:H_2O_2:H_2O$	10.7	2.11	3.5	3.5	3.1
HNO_3	12.3	2.16	3.8	3.4	3.0
$H_2SO_4:H_2O_2$	10.4	2.23	5.1	3.5	3.1
O_3 water	10.5	2.21	4.6	3.5	2.9
UVO_3/HNO_3	14.4	2.25	3.9	3.5	3.0
Error	±0.5	±0.02	±2.0	±0.1	±0.1

boiled H_2SO_4, O_3–water, and UV/O_3 treatment oxides, whose densities are as close as thermal oxide. The density of HNO_3 oxide is somewhere between these. The obtained results of the surface roughness were around 3.5 Å and almost the same for all these samples. The SiO_2/Si interface roughness, σ_I, that relates to the modulation of the interference fringe, is hard to determine accurately because of the limited number of fringes for such ultrathin films. The differences in interface roughness in Table I may be due to inaccurate fitting. The surface roughness of HF-dipped Si wafers, $\sigma_{s,HF}$, may approximately represent the interface roughness before the removal of native oxide and turned out almost the same for the various chemically treated samples. The main difference when using our method on the native oxides is the film density.

The chemical characterizations of native oxides by Fourier transform infrared (FTIR) spectroscopy and x-ray photoelectron spectroscopy (XPS) revealed that large amounts of silicon hydrides (Si–H) and silicon hydroxyls (Si–OH) exist in chemical oxides, with the exception of H_2SO_4 and UV/O_3 treated chemical oxides.[14–16] The atomic force microscopy/scanning tunneling microscopy (AFM/STM) study of the ultraviolet excited fluorine (UV/F) etched surface[17] on boiled HCl and NH_4OH formed native oxides revealed the existence of a poor-quality area in the film that is easily removed by the etching. Also, a study of the ultraviolet chlorine (UV/Cl_2) etched surface[18,19] of native oxides revealed that the O_3–water treated sample has a relatively flat surface compared to the referenced HNO_3 sample, and UV/O_3 treated samples are almost as flat as the initial surfaces.

The observed low density of the HCl and NH_4OH formed oxides may be the result of a structural imperfection in the SiO_2 due to the existence of many Si–H and Si–OH bonds that results in loosely packed native oxides. In such oxides, F or Cl radicals are easily diffused and etch the films quickly. In the case of O_3–water and UV/O_3 treated native oxides, the oxygen radicals effectively oxidize the Si–H, and Si–OH weak bonds result in the low impurity, closely packed native oxides.

IV. THERMAL OXIDES

We prepared thermal oxides with thicknesses of 40 and 70 Å. Two types of 40 Å oxides were grown thermally at 800 °C in 200 Torr O_3, where better electric properties were obtained than in O_2 ambient, starting from the Si wafer cleaned by boiled HNO_3 with and without UV/O_3 treatment discussed above. The UV/O_3 treated wafers were transferred to the load-locked oxidation furnace without being exposed to the air to avoid humidity and contamination. The heating system is a hot-walled type with 4%–5% ozone made from a discharge type ozonizer. We grew 70 Å oxides in three different ambient, 200 Torr O_2, 200 Torr O_3, and atomospheric pressure HCl/O_2 ambient at temperature between 800 and 1000 °C to see their structural differences, and measured the reflectivity for these samples.

To obtain DXR from the data, the measured reflectivity data of the Si substrate is not appropriate for R_{ave} since the surface roughness of the grown oxide and the Si substrate are not necessarily close, in contrast to the case of native oxide. Therefore, we applied the calculated reflectivity of the Si wafer with the same surface roughness as grown oxide for the average reflectivity as $R_{ave} = R_{Si,calc}(\sigma_{SiO_2})$. The standard error function was applied in the optimization since R_{ave} terms cancel out,

$$\chi^2 = \Sigma(\log_{10} R_{data} - \log_{10} R_{calc})^2/w^2.$$

In the model fitting to the reflectivity of thermal oxides, there are two possible solutions having the same interference amplitude in which the oxide density is less or more dense relative to that of the Si substrate. Figure 4 shows the calculated DXR for the 40 Å oxide whose density varied from 2.15–2.5 g/cm^3 along with the usual x-ray reflectivity for oxide with a density of 2.15 g/cm^3. From Fig. 4, the interference fringe clearly changes in the phase when the oxide density coincides with that of the Si substrate. The ambiguous solutions on density can be resolved from the shape of the first fringe at around the critical angle, ψ_c, where bumps indicate more dense oxide film and dips indicates less dense film.

In Figs. 5 and 6, typical DXRs of four samples are shown, (a) and (b) are for the 40-Å samples, (c) is for 70 Å oxide grown at 1000 °C in O_3 ambient, and (d) is for 70 Å oxide grown at 1000 °C HCl/O_2 ambient.

The broken line in Figs. 5 and 6 represents the result of the single layer model where a uniform SiO_2 on the Si substrate is assumed. From the data, the oxide density of sample (a) and (b) exceeds that of Si unlike the lower density for samples (c) and (d). However, the agreement between the

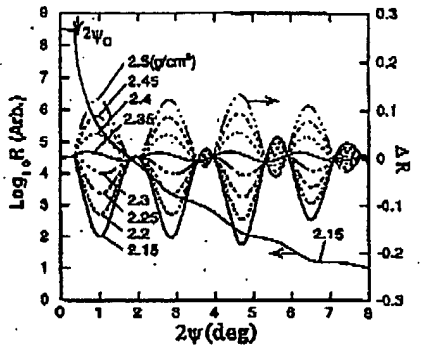

FIG. 4. Calculated difference x-ray reflectivity for 40 Å oxides. The assumed oxide densities are 2.15–2.5 g/cm³. Interference oscillation changes its phase when the oxide density exceeds that of Si (2.33 g/cm³). Original x-ray reflectivity for oxide with a density of 2.15 g/cm³ has been shown as a reference.

single layer model and the measured data is not satisfactory. The calculated DXR cannot reproduce the peak position of the oscillation and the intensity modulation precisely, and the fittings to the overall data necessitate the discrepancy of the intensity at the total reflection region below $\psi_c(=0.187°)$. In a single layer model, the difference of density between SiO_2 and Si reflects the interference amplitude. On the other hand, oxide thickness reflects the interval of the interference oscillation. The surface roughness introduces the monotonic damping of the reflectivity intensity along the incident angle. The SiO_2/Si interface roughness introduces the damping of the interference oscillation along the incident angle. From these features, these parameters are determined almost independently during the optimization. In this highly constrained

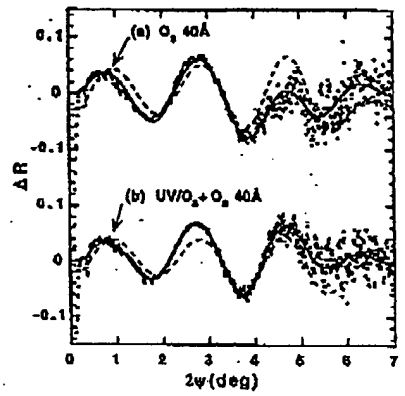

FIG. 5. Observed difference x-ray reflectivity for 40 Å oxides grown at 800 °C in O_2 ambient. Before oxidation, Si wafers are cleaned by boiled HNO_3, with the additional UV/O_2 treatment for sample (b). Broken lines indicate the results of optimization based on the single layer model. The solid line is for a two layer model which assumes a thin, dense interfacial layer at SiO_2/Si interface.

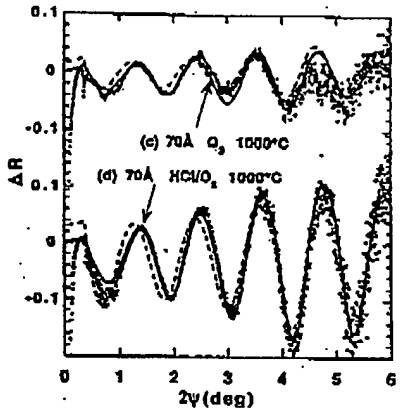

FIG. 6. Observed difference x-ray reflectivity for 70 Å oxides grown at 1000 °C in (c) O_2 ambient and (d) HCl/O_2 ambient. Broken and solid lines are the same as in Fig. 5.

single layer model, there is no room for giving such a phase the change and intensity modulation seen in the data.

By carefully analyzing the data, we found that the two-layer model with a thin, high-density interfacial layer provides quite satisfactory agreement with the data, as denoted by the solid line in the same figures. The existence of an additional thin layer introduces a wide interval oscillation that interferes with the regular oscillation from the bulk SiO_2 layer, and can reproduce the observed modulation features in the data. Such a thin, dense interfacial layer was required for all measured samples. Other combinations of parameters, such as a low-density interfacial layer or low-density surface layer, were also explored but could not reproduce the observed DXR. So, the obtained solution would be unique. The three layer model that consists of two interfacial layers did not improve the χ^2 function and the densities of these two interfacial layers are the same within their errors compared to that of the two layer model. This indicates the interfacial layer can be treated as one layer within the precision of our measurement. In the model, we assumed the chemical composition of the interfacial layer to be SiO_2. The results from the x-ray reflectivity are insensitive to the chemical elements and their chemical bondings. Actually, the δ in the complex refractive indices, which determines the shape of reflectivity, is given by $\delta=(r_0N_A/2\pi)\lambda^2\rho(Z+f')/A$, where r_0 is the classical electron radius, N_A is Avogadro's number, λ is the x-ray wavelength, ρ is the density, A is the atomic mass, and $(Z+f')$ is the atomic scattering factor. In the equation, the composition-dependent electron density $(Z+f')/A$ has values of 0.5040, 0.5046, and 0.5058, for SiO_2, SiO, and Si, respectively, at wavelength 1.3 Å. As δ is the product of this term and the density, only a 0.35% difference can be achieved for the density of the interfacial layer whether we assume SiO_2 or Si for the composition of the interfacial layer. This is because the high-energy x ray can excite all electrons in the atom whose number is close to half the

TABLE II. Extracted parameters for 40-Å-thick thermal oxides, grown at 800 °C, O_3 ambient, based on the two layer-model where the thin, dense interfacial layer exists at SiO_2/Si interface. σ_s and σ_i indicate the SiO_2 surface roughness and interface roughness at Si substrate.

	Interfacial layer			SiO_2 layer		
Pretreatment before oxidation	σ_i (Å)	Density (g/cm³)	Thickness (Å)	σ_s (Å)	Density (g/cm³)	Thickness (Å)
(a) HNO_3	1.8	2.41	14.0	4.1	2.35	25.6
(b) HNO_3+UV/O_3	2.2	2.41	12.1	4.0	2.36	28.3
Error	±2.0	±0.02	±1.0	±0.1	±0.02	±1.0

atomic number. This is in clear contrast to the optical method at long wavelengths. In this two-layer model, we set the roughness between the interfacial layer and the SiO_2 layer to 2 Å due to the large fitting error of the parameter. Results from the two layer model for 40 Å oxides are summarized in Table II. The density of the SiO_2 layer is high compared to the thick SiO_2 (~2.25 g/cm³). The difference between the two samples is in the thickness of the interfacial layer.

Figure 7 shows the evolution of the thickness of the interfacial layer on the oxidation temperature for 70 Å samples. The thickness ranged from 8–14 Å. The thickness decreases as the temperature increases. The O_2-grown oxides have the thickest interfacial layers. Oxides grown in O_3 and HCl/O_2 ambient have the thinner interfacial layers.

Figure 8 shows the densities of the interfacial layer and the SiO_2 layer versus oxidation temperature. The density of the interfacial layer is almost constant at around 2.4 g/cm³ with a slight decrease at a high oxidation temperature for O_2 and O_3 oxidation. On the bulk SiO_2 density, it decreases in the same way as that of the interfacial layers for O_2 and O_3 oxides, while it decreases much more rapidly for the HCl/O_2 oxide with the oxidation temperature.

These results are compatible, in a margin of error, with the nuclear reaction analysis using O^{18} isotopes and the thickness determination by transmission electron microscopy (TEM), where the oxide density ~2.45 g/cm³ (Ref. 20) for 810 °C, O_2 grown 29 Å oxide was deduced. Different results on a structural transition layer were reported by the grazing-incidence x-ray diffraction technique,[21] where a less dense (2.4 g/cm³) transition layer of ~70 Å exists between Si and the high density (2.6 g/cm³) bulk SiO_2 layer. However, such a high density SiO_2 layer, as dense as quartz, should give the unacceptably high refractive index of 1.55 for the optical ellipsometry[22] compared to the standard value of 1.46. This unacceptably high oxide density with a thick interfacial layer may come from the large error inherent in the estimation of x-ray penetration depth at the incident angle near the critical angle of total reflection. The density obtained by DXR technique should have small systematic errors since interference fringes depend on the difference of density to that of the Si substrate, whose densities are kept constant to 2.33 g/cm³ during optimization, in addition to the simultaneous determination of thickness, roughnesses, and the structure of samples.

V. DISCUSSION

So far, various characterizations have been performed on the SiO_2/Si system, and the experimental results have been explained by (I) the model whose interface is abrupt and has no interfacial layer,[23] (II) the model which proposes the existence of a substoichiometric (SiO_x) layer at the SiO_2/Si

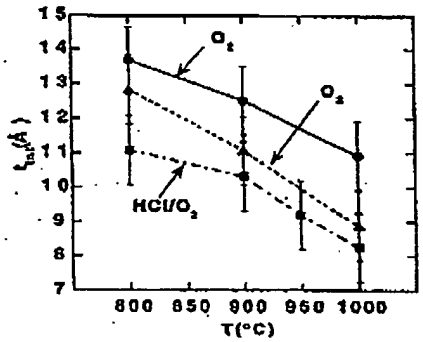

FIG. 7. Change in the thickness of the interfacial layer versus oxidation temperature for 70 Å oxides. Circle, triangle, and square correspond to the oxide grown in O_2, O_3, and HCl/O_2 ambient, respectively.

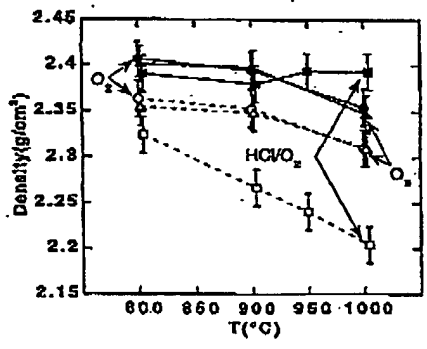

FIG. 8. Change in the density of 70 Å oxides vs oxidation temperature. Black and white marks represent the densities of the interfacial layer and the SiO_2 layer, respectively. Circles, triangles, and squares correspond to the oxide grown in O_2, O_3, and HCl/O_2 ambient, respectively.

interface,[24–26] and (III) the model in which the transitions of crystal-Si into amorphous-SiO_2 proceed via crystalline or the ordered phase of SiO_2.[27–30]

Our result clearly disagrees with the type-I model. However, our method gives no direct information on the stoichiometry or the crystallinity of the interfacial layer in the type-II and -III models. On the other hand, to explain the deviation of oxidation kinetics from the Deal–Grove model for ultrathin (<6 nm) oxides, the "reactive layer" model has been proposed[24] and developed[25] based mainly on the kinetic studies and the O (Ref. 18) labeling experiments. The reactive layer is defined as a thin (1–2 nm) oxide layer near the interface as a diffusion barrier to the interstitial O_2. The origin of the low oxygen diffusivity of the layer is considered to come from the large compressive stress at the interface. This strain produced a compact oxide with small rings or microcrystals. The density of such a compact oxide will be high compared to the bulk SiO_2. Also the crystalline polymorph of SiO_2 as tridymite, cristobalite, quartz, or coesite, has high densities ranging from 2.26–2.9 g/cm^3. These can explain the observed high density of about 2.4 g/cm^3 of the interfacial layer. Then, the observed high density interfacial layer is possibly the direct measurement of this reactive layer.

As the compact oxide or crystalline phase will be quasistable under the compressive stress, the population will decrease as the oxidation temperature increases. The observed decrease of the interfacial layer thickness along the oxidation temperature can be interpreted as the decrease of such a phase by the thermal annealing. The existence of chemically active O_3 and HCl accelerates the transition of such a phase into amorphous SiO_2, that leads to a thinner interfacial layer, in agreement with the crystal-truncation-rod (CTR) study of O_2 and O_3 grown oxides.[29] Oxides grown in HCl/O_2 ambient also have a thin, dense interfacial layer with a low density, open structure amorphous SiO_2 layer.

The electrical study of 40 Å gate oxides,[18] indicated the oxides grown from the UV/O_3-treated dense native oxide has a low surface state density (D_{it}) and small leakage current compared to that without the treatment, even in the case of same oxidation conditions. UV/O_3 treated native oxide, free from poor-quality areas associated with Si–H or Si–OH bonds, introduced the uniform oxidation layer at the Si surface whose structure remains on the interfacial layer for such ultrathin oxides. This lead to good-quality gate oxides.

On the other hand, O_3-grown oxide has superior electrical properties compared to O_2-grown oxides.[12] It is possible that ozone accelerates the phase transition of the high density phase to amorphous SiO_2 that suppresses the nonuniform growth of the high density layer at the interfacial defects of Si,[20] which leads to the uniform amorphous oxides with improved electric quality.

ACKNOWLEDGMENTS

This study was performed under the approval of the National Laboratory for High Energy Physics (Approval No. 94-Y12). The authors would like to thank the staff at Photon Factory for their cooperation with the experiment.

[1] L. G. Parrat, Phys. Rev. 95, 359 (1954).
[2] B. Vidal and P. Vincent, Appl. Opt. 23, 1794 (1984).
[3] L. Nevot and P. Croce, Rev. Phys. Appl. 15, 761 (1980).
[4] S. K. Sinha, E. B. Sirota, and S. Garoff, Phys. Rev. B 38, 2297 (1988).
[5] R. A. Cowley and T. W. Ryan, J. Phys. D 20, 61 (1987).
[6] S. M. Heald, J. K. D. Jayanetti, A. A. Bright, and G. W. Rubloff, J. Vac. Sci. Technol. A 8, 2046 (1990).
[7] Y. Horii, H. Tomita, and S. Komiya, Rev. Sci. Instrum. 66, 1370 (1995).
[8] B. L. Henke, J. C. Davis, E. M. Gullikson, and R. C. C. Perera, Lawrence Berkeley Lab. Report No. LBL-26259, 1988).
[9] S. Sasaki, KEK Report No. 88-14, 1989.
[10] J. Takano, K. Makihara, and T. Ohmi, Mater. Res. Soc. Symp. Proc. 315, 381 (1993).
[11] J. R. Vig, J. Vac. Sci. Technol. A 3, 1027 (1985).
[12] T. Nakanishi, Y. Sato, M. Okuno, and K. Takasaki, Proceedings of the Symposium VLSI Technical Digest of Technical Papers, Japan, 1994 (unpublished), p. 45.
[13] N. Awaji, Y. Sugita, S. Ohkubo, T. Nakanishi, K. Takasaki, and S. Komiya, Jpn. J. Appl. Phys. 34, L1013 (1995).
[14] H. Ogawa and T. Hattori, IEICE Trans. Electron. E75-C, 774 (1992).
[15] M. Morita, T. Ohmi, E. Hasegawa, M. Kawakami, and M. Ohwada, J. Appl. Phys. 68, 1272 (1990).
[16] Y. Sugita, N. Awaji, S. Ohkubo, S. Watanabe, S. Komiya, and T. Ito, Proceedings of the International Conference on Solid State Devices and Materials, Japan, 1995 (unpublished), p. 836.
[17] T. Aoyama, T. Yamazaki, and T. Ito, Appl. Phys. Lett. 61, 102 (1992).
[18] S. Ohkubo, Y. Tamura, R. Sugino, T. Nakanishi, Y. Sugita, N. Awaji, and K. Takasaki, Proceedings of the Symposium VLSI Technical Digest of Technical Papers, Japan 1995 (unpublished), p. 111.
[19] R. Sugino, Y. Nara, H. Horie, and T. Ito, J. Appl. Phys. 76, 5498 (1994).
[20] F. Rochhet, S. Rigo, M. Froment, C. D'Anterroches, C. Maillot, H. Roulet, and G. Dufour, Adv. Phys. 35, 237 (1986).
[21] E. Hasegawa, A. Ishitani, K. Akimoto, M. Tsukiji, and N. Ohtu, J. Electrochem. Soc. 142, 273 (1995).
[22] W. A. Pliskin, J. Vac. Sci. Technol. 14, 1064 (1977).
[23] S. Pantelides and M. Long, *Physics of SiO_2 and its Interfaces*, edited by S. Pantelides (Pergamon, New York, 1978), p. 339.
[24] A. M. Stoneham, C. R. M. Grovenor, and A. Cerezo, Philos. Mag. B 55, 201 (1987).
[25] N. F. Mott, S. Rigo, F. Rochet, and A. M. Stoneham, Philos. Mag. B 60, 189 (1989).
[26] V. A. Yakovlef, Q. Liu, and E. A. Irene, J. Vac. Sci. Technol. A 10, 427 (1992).
[27] A. Ourmazd and J. Bevk, *Physics and Chemistry of SiO_2 and the Si-SiO_2 Interfaces*, edited by C. Robert Helms and Bruce E. Deal (Plenum, New York, 1988), p. 189.
[28] B. J. Mrstik, A. G. Revesz, M. Ancona, and H. L. Hughes, J. Electrochem. Soc. 134, 2020 (1987).
[29] I. Takahashi, T. Shimura, and J. Harada, J. Phys. Condens. Matter 5, 6525 (1993).
[30] I. Takahashi, K. Nakano, J. Harada, T. Shimura, and M. Umeno, Surf. Sci. Lett. 315, L1021 (1994).

Jpn. J. Appl. Phys. Vol. 42 (2003) pp. 7493–7496
Part 1, No. 12, December 2003

Appendix B

Novel Interface Structures between Ultrathin Oxynitride and Si(001) Studied by X-Ray Diffraction

Isao TAKAHASHI*, Tositeru KADA, Kouji INOUE, Amane KITAHARA, Hiromitsu SHIMAZU, Norihisa TANAKA, Hikaru TERAUCHI, Syuichi DOI[1], Kenji NOMURA[1], Naoki AWAJI[1] and Satoshi KOMIYA[2]

Advanced Research Center of Science, Faculty of Science and Technology, Kwansei Gakuin University (ARCS-KGU), Sanda 669-1337, Japan
[1]*Fujitsu Laboratories Ltd., Morinosato-Wakamiya, Atsugi 243-0197, Japan*
[2]*Materials Science Division, Japan Synchrotron Radiation Research Institute (JASRI, SPring-8), Mikazuki-cho 679-5198, Japan*

(Received January 23, 2003; revised May 22, 2003; accepted August 27, 2003; published December 10, 2003)

For ultrathin oxynitride layers 2.4 nm thick, X-ray crystal truncation rod (CTR) scattering is conducted to investigate the interface structures between oxynitride and Si(001). (004) and (202)CTRs showed that the [amorphous oxide]/Si(001) interface is hardly varied by NO-nitrided oxynitridation. On the other hand, (111)CTR indicated that epitaxial oxide crystallites in the matrix of amorphous oxide layer are significantly affected by nitrogen: It is very likely that nitrogen atoms at the interface are captured by these crystallites after their migration on the interface. As interstitial atoms, the adsorbed nitrogen makes the crystallites amorphous. Such an annihilation of the crystallites should be responsible for the high performance of oxynitride as gate oxides. Further oxynitridation where the nitrogen concentration reaches 4 at.% showed a distinct variation in (111)CTR, indicating the creation of a novel structural order at the interface. Such a structural order is likely to be nucleated by the excessively concentrated nitrogen. A close relationship between the novel structural order and degradation of the over-oxynitrided layers is strongly suggested. [DOI: 10.1143/JJAP.42.7493]

KEYWORDS: oxynitride, Si(100) surface, gate oxide, MOSFET, X-ray diffraction, CTR scattering, nanocrystalline

1. Introduction

Continuous scaling down of silicon-based devices requires ultrathin gate oxides with high reliability. Oxynitridation is one of the promising methods for preparing ultrathin gate oxides in highly miniaturized metal-oxide semiconductor field-effect transistors (MOSFETs). Nitrogen atoms incorporated into thermal oxide layers on Si(001) substrates have been known to result in many physical properties of gate dielectrics: The density of interface traps, interface-state density, interfacial smoothness, rate of boron diffusion to the oxide, dielectric permittivity, dielectric breakdown, and leakage current density are usually improved by several appropriate oxynitridation procedures.[1–5] However, over-oxynitridation is known to degrade the gate dielectrics: Carrier mobility in the MOSFET channel is sometimes lowered and interfacial roughness is increased by an excessive amount of nitrogen.[6,7] It is a bit surprising that the variation in the interface structure has scarcely been investigated by diffraction techniques, although numerous studies concerning the atomic structure of oxynitride/Si(001) interfaces have been presented.[8–13]

X-ray scattering is a well-established technique for nondestructive structural analysis of buried interfaces. In particular, X-ray crystal truncation rod (CTR) scattering is quite sensitive to the structures of crystalline surfaces and interfaces.[14–16] Different regions of reciprocal space usually provide different kinds of information about the interface structure under examination. Therefore, by choosing the measurement regions in the reciprocal space appropriately, we can selectively observe the interfacial structure between microcrystallites and a crystalline substrate, even if an amorphous matrix occupies a major area in the interface. Actually, we have reported comprehensive CTR studies about the oxide crystallites distributed into the amorphous thermal oxide layers on Si(001) substrates[17–21] (Several results were also confirmed by other researchers.[22]):

(1) In a matrix of amorphous thermal oxide, there are crystallites that are epitaxially grown from the Si(001) substrate;
(2) Coverage of the crystallites is smaller than 10% at the interface (usually, it is several %);
(3) Stoichiometry and crystal structure have not yet been established. However, a model structure of SiO_2 type, referred to as pseudocristobalite, has been proposed which fully reproduces the observed (111)CTR with a few fitting parameters.

One of the aims of our study is to clarify the origin of the positive and negative properties of oxynitride ultrathin layers from a structural standpoint. Such a study may give us insight for a practical prescription for manufacturing reliable gate oxides less than 2 nm in thickness. In this paper, interface structures of NO-nitrided oxynitrides 2.4 nm thick on Si(001) wafers are reported: We present (004), (202) and (111)CTRs measured by synchrotron radiations so as to elucidate the change in the interface caused by incorporated nitrogen in the oxide.

2. Experimental

The substrates were p-type Si(001) wafers, the surfaces of which had been cleaned by standard cleaning procedures prior to oxidation. Wet oxidation was performed to grow an oxide layer of 2.4 nm thickness. A mixture of NO and Ar gas was adopted for oxynitridation. The oxynitridation temperature was 900°C. Nitrogen concentration was controlled by the annealing time in the oxynitridation process. Nitrogen in the oxide layer was evaluated by secondary ion mass spectroscopy: The present procedure yielded oxynitride layers with the maximum concentration of nitrogen i at.% (i=0, 1, 2, 3, 4, 5, 6). They are referred to as sample 0, sample 1, sample 2, and so on.

Two synchrotron radiation facilities were utilized for X-ray diffraction measurements: BL17A of the Photon Factory (KEK) and BL13XU at SPring-8.[23] Reflectivity and

*E-mail address: suikyo@ksc.kwansei.ac.jp

(111)CTR were collected at BL17A, and CTR scattering around the (004) position and that around the (202) position were measured at BL13XU. Reflectivities for several selected samples were also measured at BL13XU.[24] The X-ray wavelength was tuned to 0.1 nm in both experiments and all the measurements were performed at room temperature.

3. Results

Figures 1(a) and 1(b) show the integrated intensities of (004)CTR and (202)CTR; they indicated no systematic variation among the samples.[25] On the other hand, CTR scattering around the (111) position in reciprocal space exhibited complex variation, particularly in l-values ranging between 0.3 and 0.9. (111)CTRs shown in Fig. 1(c) can be classified into three groups: Samples 0 and 1, samples 2 and 3, and samples 4 and 5. By calculating the structure factor, we found that (004)CTR and (202)CTR are not very sensitive to the epitaxial crystallites.[26] However, the interfacial crystallites significantly affect the (11l)CTR at l-values between 0.3 and 0.9. Consequently, (004)CTR and (202)CTR mainly afford the structure of the [amorphous oxide]/Si(001) interface, whereas we can obtain information on the structure of the [epitaxial pseudocristobalite crystallites]/Si(001) interface by measuring the (111)CTR.

In previous studies of thicker oxide layers, *i.e.*, thermal oxide films of 20–80 nm thickness, a distinct intensity enhancement at the (11l_{max}) position, where l_{max} is usually between 0.4 and 0.5, as well as *Laue*-function-like fringes around the (11l_{max}) were observed.[17–20] Since this (11l_{max}) reflection is indexed as the (101) Bragg reflection of epitaxial pseudocristobalite, the l_{max}-value simply represents the inverse of the lattice parameter of pseudocristobalite in the direction normal to the interface, conventionally referred to as the c-axis length in the tetragonal lattice. According to our previous studies, $\Delta(l_{max})\equiv$[{(11l_{max}) reflection intensity} − {(11l)CTR intensity from a Si(001) at $l=l_{max}$}] reflects the volume fraction of the pseudocristobalite crystallites in the oxide layer. If we recall the thickness of the ultrathin oxide layers in this study (2.4 nm) and the c-axis length of pseudocristobalite (1.2–1.3 nm), no clearly resolved peaks around (11l_{max}) should be expected; only a broad hump or shoulder may be observed near the (11l_{max}) position. Nevertheless, by evaluating $\Delta(l_{max})$ we can estimate the coverage of the crystallites at the interface even in the case for the ultrathin layers investigated in this study.

4. Discussion

For the ultrathin oxynitride layers, the coverage of the interfacial crystallites can be proportional to $\Delta_i(l) \equiv I_i^{\mathrm{CTR\_OBS.}}(l) - I_{\mathrm{Si}}^{\mathrm{CTR\_CAL.}}(l)$ around l=0.5, where $I_i^{\mathrm{CTR\_OBS.}}(l)$ is the observed (11l)CTR intensity of sample i, and $I_{\mathrm{Si}}^{\mathrm{CTR\_CAL.}}(l)$ is the calculated (11l)CTR intensity scattered from a Si(001) surface.[27] $I_{\mathrm{Si}}^{\mathrm{CTR\_CAL.}}(l)$ is shown in Fig. 2(a) by solid curves. In Fig. 2(b), there is a broad peak in $\Delta_1(l)$ and $\Delta_0(l)$ around l=0.57 which is close to l_{max} of the thicker oxides we have observed. We consider that these broad peaks indicate the existence of the crystallites in the ultrathin oxynitride (sample 1), as well as in the ultrathin thermal oxide (sample 0). Fitting procedures to $I_i^{\mathrm{CTR\_OBS.}}(l)$ based on our pseudocristobalite model successfully converged only for samples 0 and 1. The refined parameters are listed in Table I and the best-fit calculations are also shown in Fig. 1(c) as solid curves (the program was the same as that

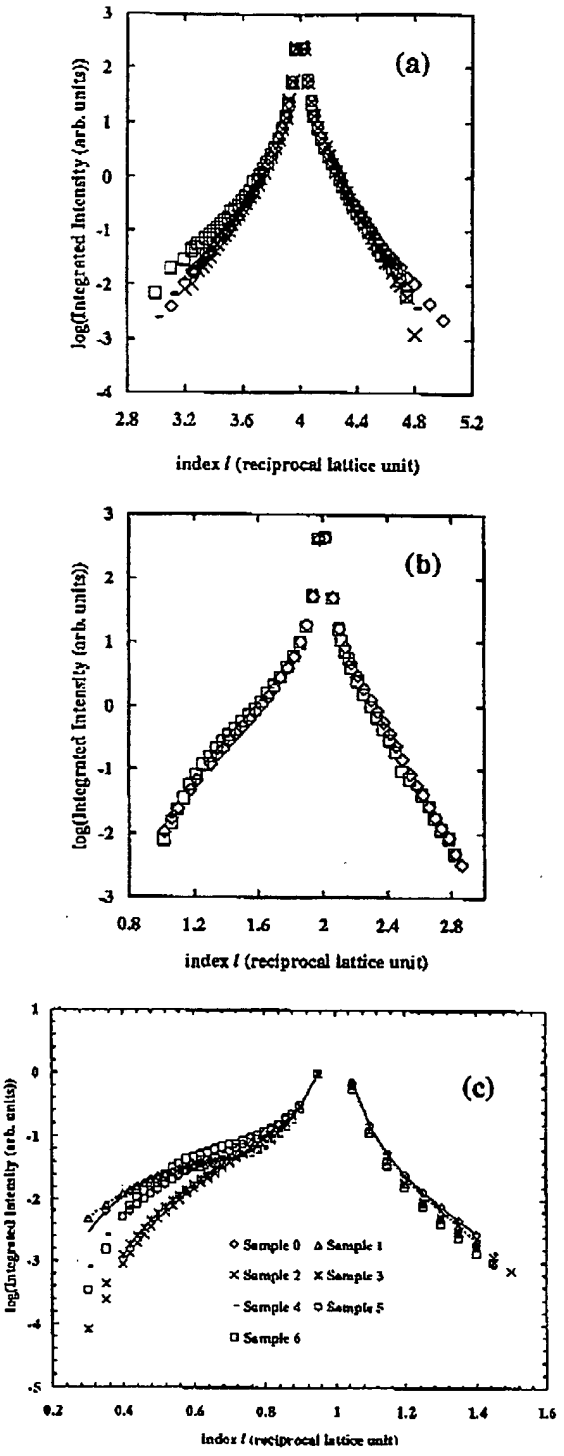

Fig. 1. (004)CTR of samples 0, 2, 4 and 6 (a), (202)CTR of samples 0 and 6 (b), and (111)CTR of samples 0, ..., 5 (c), scattered from the interfaces between the ultrathin oxynitride and Si(001). Definition of sample i (i = 0, ..., 6) is written in the text. For samples 0 and 1, the best-fit calculation based on the epitaxial pseudocristobalite model is indicated as solid curves. The fitted parameters are listed in Table I.

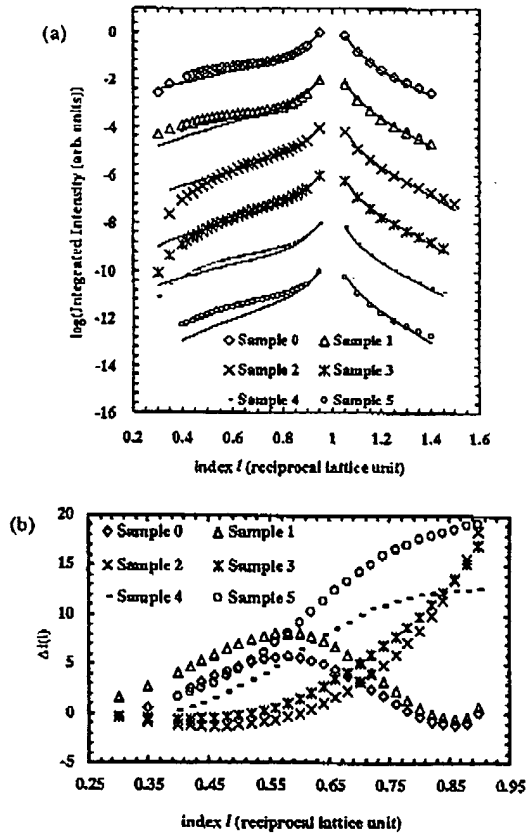

Fig. 2. $I_i^{CTR\_OBS.}(l)$, $I_{Si}^{CTR\_CAL.}(l)$ (a), and $\Delta_i(l)$ (b), for sample i (i=0,...,5). Definitions of $I_i^{CTR\_OBS.}(l)$, $I_{Si}^{CTR\_CAL.}(l)$ and $\Delta_i(l)$ are described in the text. In order to calculate $I_{Si}^{CTR\_CAL.}(l)$, scale and roughness parameters were fitted by using the data with the l-value greater than 0.9 in which the structure factor of pseudocristobalite is negligible. Fitted roughness parameters σ [nm] and estimated standard deviations (listed in parentheses) are 0.11(0.02) for sample 0, 0.16(0.02) for sample 1, 0.16(0.07) for sample 2, 0.18(0.07) for sample 3, 0.13(0.06) for sample 4, and 0.22(0.08) for sample 5. For clarity, $I_i^{CTR\_OBS.}(l)$ (symbols) and $I_{Si}^{CTR\_CAL.}(l)$ (solid curves) of different samples are displaced vertically in (a). For samples 0 and 1, broad peaks are indicated in $\Delta_i(l)$ around l=0.57, whereas no peak is seen for samples 2 and 3 in this range. A broad hump in $\Delta_i(l)$ appears again for samples 4 and 5 where the center of the hump is shifted to a larger l-value, although the peak profile is not resolved here.

Table I. Fitted parameters of sample 0 and sample 1. Discrepancy factor R is given as $\Sigma|\ln I^{Obs.}(l) - \ln I^{Cal.}(l)|/\Sigma|\ln I^{Obs.}(l)|$ where $I^{Obs.}(l)$ and $I^{Cal.}(l)$ are the observed (11l)CTR and calculated (11l)CTR based on the pseudocristobalite model. Coverage ρ represents the area fraction of pseudocristobalite in the interface. c is the lattice parameter of pseudocristobalite crystallites. σ represents the root mean square roughness of the interface. The estimated standard deviations (ESDs) obtained by the least-squares routine are indicated in parentheses.

	R	ρ (%)	c [nm]	σ [nm]
Sample 0	0.009	0.73(0.03)	1.27(0.01)	0.13(0.01)
Sample 1	0.014	0.90(0.02)	1.28(0.02)	0.18(0.01)

used by us in refs. 18–20; the number of the unit cell of pseudocristobalite stacked in the direction normal to the interface (denoted P_{max} in ref. 18 was fixed to be one, since the assumption $P_{max}>1$ did not give any sufficient fittings). Thereby, we conclude that the oxynitride layer still holds the epitaxial crystallites at the initial stage of oxynitridation even if the thickness of the oxynitride layer is comparable to the c-axis length.

For samples 2 and 3, no enhancement is seen in $\Delta_2(l)$ and $\Delta_3(l)$ in this range, indicating annihilation of the crystallites in these oxynitride layers. The least-squares routine performed for the corresponding data sets shown in Fig. 1(c) did not show any indication of the epitaxial crystallites for these samples, either. Hence, there is no doubt that further oxynitridation where the nitrogen concentration reaches 2 at.% causes the annihilation of the interfacial crystallites. Two important results were obtained in this study: (i) nitrogen concentration of 2 at.% is sufficient to destroy almost all the interfacial crystallites; (ii) the [amorphous oxide]/Si(001) interface is hardly changed by the nitrogen incorporated, which is indicated from the negligible variation between sample 0 and sample 2 in (004)CTR [Fig. 1(a)]. The results (i) and (ii) lead us to an interesting speculation: we consider that the stable sites for the incorporated nitrogen are within the epitaxial crystallites, and the nitrogen in the crystallites destroys the host pseudocristobalite crystallites in the end. A drastic volume expansion due to nitrogen incorporation may transform the crystallites into amorphous.

For samples 4 and 5, one more interesting feature was revealed: (111)CTRs of samples 4 and 5 have a shoulder similar to samples 0 and 1 [Fig. 1(c)]. However, the shoulder shifts at higher angles than those of samples 0 and 1, indicating the shrinkage of the c-axis length. The least-squares fittings of (111)CTR exhibited a tendency to give a c-axis length of the crystallites less than 0.8 nm for samples 4 and 5, although these fittings have never converged successfully. $\Delta_4(l)$ and $\Delta_5(l)$ shown in Fig. 2(b) would also support the perspective, i.e., the center of the broad hump in $\Delta_4(l)$ and $\Delta_5(l)$ shifts to larger l-values than those of $\Delta_0(l)$ and $\Delta_1(l)$. Since shrinkage in lattice constant from 1.27 nm to 0.8 nm without changing the crystal structure is hardly acceptable and we have observed the disappearance of pseudocristobalite crystallites in samples 2 and 3, it is natural for us to consider that another crystalline order is formed at the interface by further oxynitridation. If such a change is triggered by oxynitridation, excess nitrogen at the interface should act as nuclei for the novel structural order.

The disappearance of the epitaxial crystallites and the formation of the novel structural order in the interface should be responsible for the various, complex variations of the physical properties of the oxynitrides reported. We think that the annihilation of the pseudocristobalite crystallites can be the origin of the improved performance of oxynitride as gate oxides, since such microcrystallites at the interface can increase the interface state density as well as the interfacial roughness; the concept that a leakage current tends to flow through the crystallites is highly appealing to the authors. On the other hand, the novel structural order observed in the over-oxynitrided samples (for samples 4 and 5) can be the origin of the degradation of gate dielectrics: The structural order at the interface as a form of atomic clusters may slightly roughen the interface and increase strains at the interface; it can lower the channel mobility by increasing the scattering probability of carriers. Relationships among the decay of the epitaxial crystallites, formation of the novel

structural order, and evolution of many physical properties of oxynitride layers constitute an important subject that should be intensively studied for manufacturing MOSFETs in the near future.

5. Summary

We have investigated the interface structures between oxynitride ultrathin layers and Si(001) by synchrotron radiations. As the most striking result, the interfacial crystallites revealed annihilation as oxynitridation proceeds, implying that the nitrogen atoms are selectively absorbed by the interfacial crystallites and the crystallites are destroyed by the interstitial nitrogen in the end. The formation of a new ordering structure at the interface was strongly suggested in the case of the higher nitrogen concentration, although we did not construct any structural model for it. We consider that the excessive incorporation of nitrogen at the first interfacial layer can be the nuclei of the novel structural order.

Acknowledgements

We would like to thank Dr. O. Sakata and Dr. Y. Yoda for their tremendous help and important advice during the experiments at SPring-8. This study was financially supported by the Ministry of Education, Culture, Sports, Science and Technology of Japan (No. 11874055), and *Fujitsu Laboratories Ltd.* Proposal numbers of the Photon Factory and SPring-8 are 2000G053 and 2000B0230-ND-np, respectively.

1) S. T. Chang, N. M. Johnson and S. A. Lyon: Appl. Phys. Lett. 44 (1984) 316.
2) G. Y. Yoon, A. B. Yoshi, J. Kim and D. L. Kwong: IEEE Electron Device Lett. 14 (1993) 179.
3) W. Ting, H. Wang, J. Lee and D. L. Kwong: Appl. Phys. Lett. 57 (1990) 2808.
4) M. Bhat, J. Kim, J. Yan, G. W. Yoon, L.-K. Han and D. L. Kwong: IEEE Electron Device Lett. 15 (1994) 421.
5) M. L. Green, D. Brasen, K. W. Evans-Lutterodt, L. C. Feldman, K. Krisch, W. N. Lennard, L. Manchanda and M.-T. Tang: Appl. Phys. Lett. 65 (1994) 848.
6) M. Takayanagi-Takagi and Y. Toyoshima: IEDM Tech. Dig., 1998, p. 575.
7) K. Inoue, K. Furuno, H. Kato, N. Tamura, K. Hikazutani, S. Sano and T. Hattori: Jpn. J. Appl. Phys. 40 (2001) L539.
8) A. Kamath, D. L. Kwong, Y. M. Sun, P. M. Blass, S. Whaley and J. M. White: Appl. Phys. Lett. 70 (1997) 63.
9) G. -M. Rignanese, A. Pasquarello, J. C. Chalier, X. Gonze and R. Car: Phys. Rev. Lett. 79 (1997) 5174.
10) G. -M. Rignanese and A. Pasquarello: Phys. Rev. B 63 (2001) 075307.
11) J. P. Chang, M. L. Green, V. M. Donnelly, R. L. Opila, J. Eng, Jr., J. Sapjeta, P. J. Siverman, B. Weir, H. C. Lu, T. Gustafsson and E. Garfunkel: J. Appl. Phys. 87 (2000) 4449.
12) Z. Jing, G. Lucovsky and J. L. Whitten: J. Vac. Sci. & Technol. B 13 (1995) 1613.
13) S. Jeong and A. Oshiyama: Phys. Rev. Lett. 86 (2001) 3574.
14) S. R. Andrew and R. A. Colley: J. Phys. C 18 (1985) 6427.
15) I. K. Robinson: Phys. Rev. B 33 (1986) 3830.
16) N. Kashiwagura, Y. Kashihara, M. Sakata, J. Harada, S. W. Wilkins and A. W. Stevenson: Jpn. J. Appl. Phys. 26 (1987) L2026.
17) Y. Iida, T. Shimura, J. Harada, S. Samata and Y. Matsushita: Surf. Sci. 258 (1991) 235.
18) I. Takahashi, T. Shimura and J. Harada: J. Phys.: Condens. Matter 5 (1993) 6525.
19) I. Takahashi, K. Nakano, J. Harada, T. Shimura and M. Umeno: Surf. Sci. 315 (1994) L1021.
20) I. Takahashi, S. Okita, N. Awaji, Y. Sugita and S. Komiya: Physica B 245 (1998) 306.
21) N. Awaji, Y. Sugita, Y. Horii and I. Takahashi: Appl. Phys. Lett. 74 (1999) 2669.
22) A. Munkholm, S. Brennan, F. Comin and L. Ortega: Phys. Rev. Lett. 75 (1995) 4254.
23) O. Sakata, *et al.*: Surf. Rev. Lett. 10 (2003) 543.
24) The reflectivity of sample 0 was fitted by a three-layer model: a Si substrate (density of the substrate ρ_{Si} was fixed to be 2.33 g/cm^3); an interfacial oxide layer (L1); and an uppermost oxide layer (L2). The fitted parameters were $\sigma_{Si\text{-}L1}$=0.2(0.2) nm, ρ_{L1}=2.30(0.03) g/cm^3, d_{L1}=1.5(0.1) nm, $\sigma_{L1\text{-}L2}$=0.2(0.2) nm, ρ_{L2}=1.98(0.03) g/cm^3, d_{L2}=0.8(0.1) nm, and σ_{L2}=0.2(0.2) nm. Here, $\sigma_{Si\text{-}L1}$ denotes roughness between the Si substrate and the interfacial layer, ρ_{L1} and d_{L1} are the density and thickness of the interfacial layer, and $\sigma_{L1\text{-}L2}$ is roughness between the interfacial layer and the uppermost layer. ρ_{L2}, d_{L2} and σ_{L2} are the density, thickness and surface roughness of the uppermost layer, respectively. The ESDs are indicated in parentheses. Note that $d_{L1}+d_{L2}$(=2.3 nm) is close to the thickness of the thermal oxide (=2.4 nm) measured by ellipsometry.
25) Critical observation of Fig. 1(a) reveals a difference between the (004)CTR of sample 6 and the others, which might suggest that the interfacial roughness of sample 6 is fairly small. However, the authors do not consider that this change originates from the variation of the interface structure, since the difference between the (202)CTR of sample 6 and that of sample 0 is still negligible [Fig. 1(b)]. The observed change in sample 6 in (004)CTR can originate from the variation of the oxide overlayer, since any variation of amorphous overlayers affects the extended reflectivity, such as (004)CTR.
26) Unlike the case of ref. 18 where the coverage of pseudocristobalite was about 10%, the structure factor of pseudocristobalite around (202) and (004) is too small to yield any observable intensity enhancement in these regions in the present study, where the coverage is less than 1%. The lower angle regime of the observed (202)CTR appears to indicate some intensity enhancement such as that of (111)CTR. However, it is fully explained by the behavior of the resolution function, an effect of the illuminating area of the incident X-ray beam, and the l-dependence of the structure factor of Si crystal $F_{Si}(20l)$: We do not need the crystallites for reproducing this observed enhancement.
27) In refs. 18–21, total intensity along the (11l) line was analyzed by a model in which the total structure factor $<\Phi(l)>$ was defined as $<\Phi_{Si}(l)> + <\Phi_{PC}(l)>$, where $<\Phi_{Si}(l)>$ is the structure factor of the Si substrate and $<\Phi_{PC}(l)>$ is that of the pseudocristobalite crystallites proportional to the density of the crystallites ρ. For the ultrathin oxide layer discussed in this study, we can regard ρ as the coverage of the pseudocristobalite at the interface. Moreover, $\Delta_l(l) \equiv I_l^{CTR\_OBS.}(l) - I_{Si}^{CTR\_CAL.}(l)$ being equal to $|<\Phi(l)>|^2 - |<\Phi_{Si}(l)>|^2 = |<\Phi_{PC}(l)>|^2 + <\Phi_{PC}(l)>^* <\Phi_{Si}(l)> + <\Phi_{PC}(l)> <\Phi_{Si}(l)>^*$ should be proportional to ρ, since $|<\Phi_{PC}(l)>|^2$ ($\propto \rho^2$) is much smaller than $<\Phi_{PC}(l)>^* <\Phi_{Si}(l)> + <\Phi_{PC}(l)> <\Phi_{Si}(l)>^*$ ($\propto \rho$) for very small ρ.